Monthly Notices of the ROYAL ASTRONOMICAL SOCIETY

MNRAS **526,** 750–757 (2023) https://doi.org/10.1093/mnras/stad2758
Advance Access publication 2023 September 12

Search for particle acceleration in two massive Wolf–Rayet stars using uGMRT observations

Anindya Saha [1]★ Anandmayee Tej [1]★ Santiago del Palacio [2] Michaël De Becker,[3] Paula Benaglia,[4] C. H. Ishwara-Chandra[5] and Prachi Prajapati[6]

[1]*Indian Institute of Space Science and Technology, Thiruvananthapuram 695 547, Kerala, India*
[2]*Department of Space, Earth and Environment, Chalmers University of Technology, SE-412 96 Gothenburg, Sweden*
[3]*Space sciences, Technologies and Astrophysics Research unit – STAR, University of Liège , Quartier Agora, 19c, Allée du 6 Août, B5c, 4000 Sart Tilman, Belgium*
[4]*Instituto Argentino de Radioastronomía (CCT La Plata, CONICET; CICPBA; UNLP), C.C.5, (1894) Villa Elisa, Buenos Aires, Argentina*
[5]*National Centre for Radio Astrophysics, Tata Institute of Fundamental Research, Pune University Campus, Ganeshkhind, Pune 411007, India*
[6]*Physical Research Laboratory (PRL), Navrangpura, Ahmedabad 380 009, Gujarat, India*

Accepted 2023 September 8. Received 2023 September 8; in original form 2023 June 23

ABSTRACT

Large wind kinetic power of Wolf-Rayet (WR) stars make them ideal targets in low radio frequencies to search for non-thermal emission due to relativistic particle acceleration. In this paper, we present observations of two WR stars, WR 114 and WR 142, in Band 4 (550–950 MHz) and Band 5 (1050–1450 MHz) using the upgraded Giant Meterwave Radio Telescope. Neither star is detected in the observed frequency bands, nor extended emission associated with them. The upper limit to the free–free radio emission from the stellar wind enables us to constrain the mass-loss rate of WR 114 to $\lesssim 10^{-5}\,M_{\odot}\,yr^{-1}$; this is a factor three smaller than previously estimated using spectroscopic modelling. If we further assume that the WR stars are binaries, the non-detection of synchrotron emission from the putative wind collision region implies that the stars are either in very wide binary systems away from periastron, or that the stars are in close binary systems with an orbital separation <70 AU for WR 114 and <20 AU for WR 142. The non-detection of low-frequency radio emission from these two systems thus provides evidence that narrows their nature, though it does not rule them out as bona fide particle-accelerating colliding-wind binaries.

Key words: radiation mechanisms: non-thermal – radiation mechanisms: thermal – stars: Wolf–Rayet – radio continuum: ISM – stars: individual: WR 114 and WR 142.

1 INTRODUCTION

Studies of massive stars are of prime importance in stellar astrophysics given their strong mechanical, radiative, and chemical feedback. In particular, their intense radiation field expels and accelerates the outer layers of the star, giving rise to powerful supersonic winds. These winds deposit a large amount of mechanical energy into the interstellar medium (ISM) generating strong adiabatic shocks suitable for relativistic particle acceleration, presumably via diffusive shock acceleration (DSA; e.g. Drury 1983, and references therein). Detection of non-thermal (NT) radio emission, which is synchrotron radiation produced by relativistic electrons in the presence of a magnetic field (Blumenthal & Gould 1970; White 1985), is an observational evidence of particle acceleration.

About 50 NT radio-emitting binary systems, referred to as particle-accelerating colliding-wind binaries (PACWBs), have been identified[1] (De Becker & Raucq 2013). It is not clear how efficient these systems are at converting wind kinetic energy into particle acceleration, but at least for the WR binary Apep, it was recently shown that this fraction can be close to 1 per cent (del Palacio et al. 2023), while for WR 146 it can be as high as 30 per cent (Pittard, Romero & Vila 2021). In an observational breakthrough, NT radio emission from the stellar bubble G2.4+1.4, associated with the presumably single WR star WR 102, was detected by Prajapati et al. (2019). In this case, the fraction of the kinetic wind power that is converted into cosmic-ray acceleration was estimated to be of the order of a few per cent. Further, NT radio emission has also been detected in bow shocks of massive runaways stars (Benaglia et al. 2010; Moutzouri et al. 2022). For the runaway star BD+43 3654, Benaglia et al. (2021) estimated that ∼10 per cent of the wind kinetic power should be converted into relativistic particle acceleration in the bow shock. These observations support the hypothesis that massive stars are relevant sources of Galactic cosmic rays, as estimated by Seo, Kang & Ryu (2018) under the assumption that typically 1–10 per cent of their wind luminosity is transferred to relativistic particles. Moreover, WR stars can also be key to explain the composition of cosmic rays (Gabici 2023, and references therein).

The energy budget for NT particle acceleration depends on the wind kinetic power, $P_{\rm kin}$. For a star with mass-loss rate $\dot{M}$ and terminal velocity v_{∞}, it is $P_{\rm kin} \approx 0.5\,\dot{M}\,v_{\infty}^2$. In addition, under certain assumptions, the efficiency of particle acceleration scales

★ E-mail: anindya.s1130@gmail.com (AS); tej@iist.ac.in (AT)
[1]Updated PACWB catalogue can be found at https://www.astro.uliege.be/~debecker/pacwb/

Table 1. Parameters of WR 114 and WR 142.

	WR 114	WR 142
RA (J2000)	$18^h23^m16.3^s$	$20^h21^m44.3^s$
DEC (J2000)	$-13°43'26.1''$	$+37°22'30.5''$
Spectral type[a]	WC5	WO2
Distance (D; kpc)[b]	1.97 ± 0.09	1.68 ± 0.04
μ_α (mas yr^{-1})[b]	0.12 ± 0.03	-3.44 ± 0.01
μ_δ (mas yr^{-1})[b]	-1.99 ± 0.02	-6.37 ± 0.01
T_* (kK)[c]	79	200
R_* ($R_\odot$)[c]	2.68	0.80
$\dot{M}$ ($M_\odot$ yr^{-1})[c]	3.1×10^{-5}	1.6×10^{-5}
v_∞ (km s^{-1})[c]	3200	5000
$P_{\rm kin}$ (erg s^{-1})	1.0×10^{38}	1.3×10^{38}

Note. [a]Smith (1968) for WR 114, Barlow (1982) and Kingsburgh, Barlow & Storey (1995) for WR 142; [b]*Gaia* DR3 data (Gaia Collaboration 2022); [c]Sander et al. (2019).

with the square of the shock (and therefore the wind) velocity (Drury 1983). WR stars, which are the evolved counterparts of O-type stars, have high mass-loss rates $\sim(1–5) \times 10^{-5}\,M_\odot\,yr^{-1}$ (e.g. Abbott et al. 1986; Leitherer, Chapman & Koribalski 1997; Chapman et al. 1999) and fast winds with velocities ranging between ∼700 and 6000 km s^{-1} (e.g. Nugis et al. 1998; Hamann, Koesterke & Gräfener 2000; Nugis & Lamers 2000). Thus, their winds are exceptionally powerful with a typical $P_{\rm kin} > 10^{37}$ erg s^{-1}. This amounts to substantial mechanical energy available to drive particle acceleration, thus making this subset of hot and massive stars ideal targets to search for particle acceleration.

The requirement of large $P_{\rm kin}$ sets the primary target selection criteria for this radio investigation of particle acceleration in massive WR stars. Furthermore, there is growing observational evidence of a strong correlation between the detection of NT emission and binarity in O-type and WR systems (e.g. De Becker & Raucq 2013). In comparison, detection of NT emission in low radio frequency is reported for only one presumably single non-runaway star system (WR 102; Prajapati et al. 2019). This detection opens a new window to probe shock physics and assess the role of the local ISM and its interaction with the powerful WR winds as a necessary ingredient for particle acceleration in single massive stars.

With the aim to explore the above two scenarios, we carried out low-frequency (735 and 1260 MHz) radio observations of WR 114 and WR 142, two nearby (distance $\lesssim 2$ kpc) WR stars with large wind kinetic power ($\sim 10^{38}$ erg s^{-1}). Following the discussion in Benaglia et al. (2021), we derived the tangential velocities of these two stars with respect to its local ISM from the latest proper motion values listed in *Gaia* DR3 data base (see Table 1). The estimated tangential velocities are 10.2 and 18.0 km s^{-1} for WR 114 and WR 142, respectively, implying that these are not runaway stars (e.g. Eldridge, Langer & Tout 2011). The coordinates and relevant parameters of these stars are listed in Table 1. Located in the Ser OB1 association, WR 114 is classified as WC5 spectral type. Comparing the strength of emission lines with those in other stars of the same spectral type, van der Hucht (2001) proposed the presence of an OB companion. However, the Potsdam WR spectral modelling was consistent with a single star (Sander, Hamann & Todt 2012). WR 114 was observed with *XMM–Newton* (Oskinova et al. 2003). The non-detection of X-ray emission ($L_{\rm X} \lesssim 2.5 \times 10^{30}$erg s^{-1}) was attributed to the high opacity of the metal-rich and dense wind from the WC star. The other target, WR 142 (spectral type WO2), belongs to the Berkeley 87 cluster and is one of the only four WO stars detected in our Galaxy. *XMM–Newton* and *Chandra* observations reveal weak X-ray emission with excess absorption below 2 keV (Sokal et al. 2010). These authors discussed several possible emission processes, including thermal and non-thermal ones (e.g. inverse-Compton scattering) and a possible colliding-wind shock scenario, to interpret their observations, but their results were not conclusive.

This paper is organized as follows. The observations and data reduction procedure are described in Section 2. After reporting on the main results in Section 3, we detail in Section 4 the scientific discussion of the two WR stars in the framework of the scenarios introduced above. Our main conclusions are finally provided in Section 5.

2 OBSERVATIONS AND DATA REDUCTION

We probed the radio continuum emission associated with WR 114 and WR 142 using the upgraded Giant Meterwave Radio Telescope (uGMRT) situated in Pune, India. GMRT offers a Y-shaped array configuration of 30 fully steerable antennas of 45-m diameter. The central square km houses 12 randomly placed antennas and the remaining 18 antennas are uniformly distributed in the arms, with 6 on each arm. With this hybrid array arrangement, GMRT provides largest and smallest baselines of 25 km and 100 m, respectively, which makes it capable of probing radio emission at both small and large spatial scales. The largest detectable structures in Band 4 and 5 are 17 and 7 arcmin, respectively.[2] Details of the GMRT system can be found in Swarup et al. (1991) and Gupta et al. (2017).

Dedicated observations (Project code: 38_070) were carried out for both sources in Band 4 (550–950 MHz) and Band 5 (1050–1450 MHz) with the GMRT Wideband Backend (GWB) correlator configured to have a bandwidth of 400 MHz across 4096 channels. Primary calibrators were observed at the beginning and end of the observation for flux and bandpass calibration. The phase calibrators were observed after each scan (30 min) of the target to calibrate the phase and amplitude variations over the entire observing period. Details of the observations are given in Table 2.

The data reduction process of flagging, calibration, imaging, and self-calibration was done using the CAPTURE[3] continuum imaging pipeline for uGMRT (Kale & Ishwara-Chandra 2021), which utilizes tasks from Common Astronomy Software Applications (CASA; McMullin et al. 2007). The Perley & Butler (2017) scale was employed to set the flux density calibration. After the initial rounds of editing and calibration, we used the multiterm multifrequency synthesis (MT-MFS; see Rau & Cornwell 2011) algorithm in the *tclean* task to account for possible deconvolution errors in wide-band imaging. In the pipeline, five rounds of phase-only self-calibration were performed before making the final image. These maps were then corrected for primary beam gain. All images used in our analysis are primary beam corrected.

3 RESULTS

The radio maps of WR 114 and WR 142 are shown in Figs 1 and 2, respectively. In these maps the positions of the WR stars and other known radio sources are marked. The details of the maps (resolution and *rms*) are listed in Table 2. The maps presented in the figures have been convolved with a beam size of 5.0 arcsec.

[2]GMRT Observer's Manual (http://www.ncra.tifr.res.in/ncra/gmrt/gmrt-users/observing-help/manual_7jul15.pdf)
[3]https://github.com/ruta-k/CAPTURE-CASA6.git

Table 2. Details of observations and the obtained radio maps.

	WR 114		WR 142	
	Band 4 (550–950 MHz)	Band 5 (1050–1450 MHz)	Band 4 (550–950 MHz)	Band 5 (1050–1450 MHz)
Observation date	27/08/2020	26/06/2020	24/06/2020	22/06/2020
Flux calibrator	3C48, 3C286	3C48, 3C286	3C48	3C48
Phase calibrator	1822−096	1911−201	2052+365	2052+365
Angular resolution	4.3 arcsec ×3.4 arcsec	2.7 arcsec ×1.6 arcsec	4.1 arcsec ×3.3 arcsec	2.3 arcsec ×1.8 arcsec
rms (μJy beam^{-1})	41	22	37	32

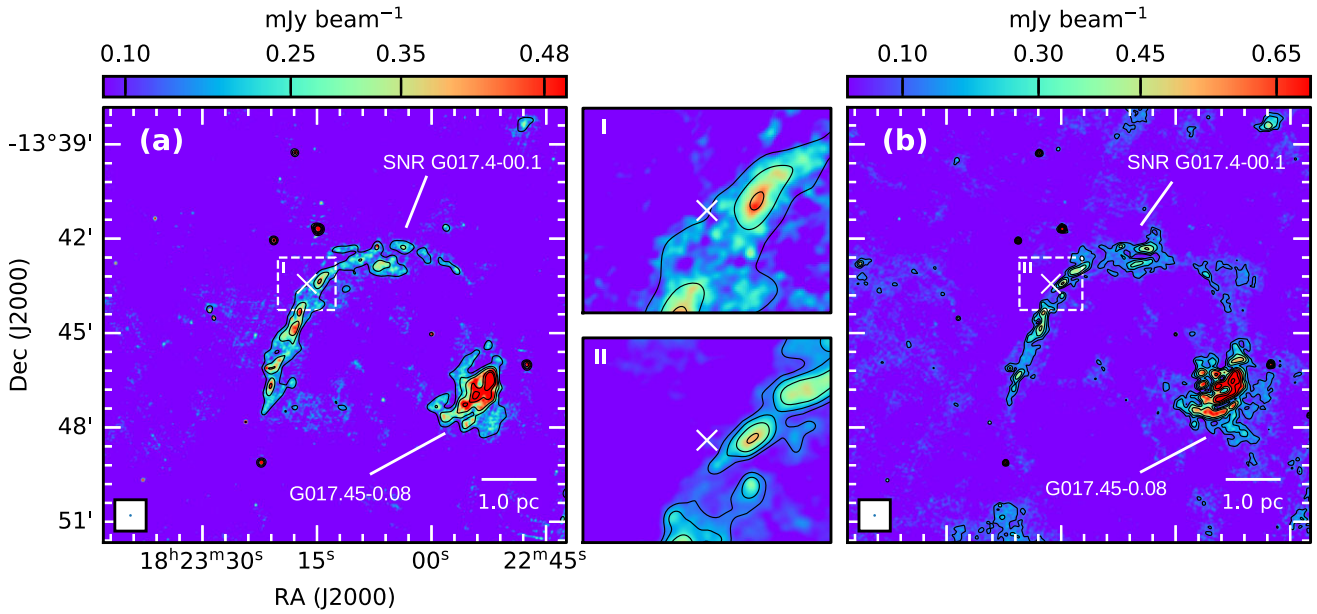

Figure 1. Radio maps of the region around WR 114, obtained using uGMRT GWB data. Both maps are convolved to a circular beam of size 5.0 arcsec. The white cross (×) in all panels shows the position of WR 114. (a) Map at Band 4 (550−950 MHz). The colourscale indicates the flux density. The black contours overlaid correspond to the levels of 0.1, 0.2, 0.3, 0.5, 0.7 mJy beam^{-1}. Zoomed in view of the region closer to the WR star (marked I) is also shown. (b) Same but for Band 5 (1050–1450 MHz). The contours correspond to the levels of 0.1, 0.2, 0.3, 0.5, 0.7, 1.0, 1.4 mJy beam^{-1}. In all panels, the contours are smoothed over 5 pixels using a Gaussian kernel. The locations of the SNR and H II region are marked. Zoomed in view of the region closer to the WR star (marked II) is also shown.

There is no radio emission detected for these stars in the observed frequency bands. Of particular mention is the field of WR 114: The Band 4 map shows faint, diffuse emission at the location of the WR star. However, this emission is most likely part of an arc-like structure associated with the supernova remnant (SNR) SNR G017.4−00.1 (Brogan et al. 2006; Green 2009) in the background along the line-of-sight towards WR 114, at an estimated distance of 18.6 kpc (Pavlović et al. 2013). Other radio sources detected in both fields are marked in the respective figures. Thus, these maps give only upper limits to the flux density from the stars. From the achieved *rms* level of the uGMRT maps, for WR 114 we derive 3σ upper limits of 123 μJy ($\nu L_\nu < 4.2 \times 10^{26}$ erg s^{-1}) and 66 μJy ($\nu L_\nu < 3.9 \times 10^{26}$ erg s^{-1}) at 735 and 1260 MHz, respectively. For WR 142, the upper limits are 111 μJy ($\nu L_\nu < 2.8 \times 10^{26}$ erg s^{-1}) and 96 μJy ($\nu L_\nu < 4.1 \times 10^{26}$ erg s^{-1}) at 735 and 1260 MHz, respectively.

Both WR stars have been previously observed at higher frequencies. In their search for radio emission towards WR stars, Chapman et al. (1999) presented ATCA observations of WR 114. No emission was detected in none of the observed frequency bands. Both WR stars are also undetected in a VLA 6 cm observation presented by Abbott et al. (1986). In addition, Cappa, Goss & van der Hucht (2004) observed WR 114 and WR 142 at 3.6 cm as part of a VLA survey of Galactic WR stars. In their study, WR 114 is classified as a probable detection (with signal-to-noise ratio of ≈4), whereas WR 142 is listed as non-detection. It is to be noted that these authors advocate further confirmation of probable detections. Additionally, given the beam size (9 arcsec × 6 arcsec) of these observations, there could be contribution from the background SNR. The 3σ upper limits from the above studies along with the ones obtained in this work are compiled in Table 3.

4 DISCUSSION

4.1 Size of the stellar wind photosphere

The stellar winds consist of ionized gas with a density profile that decreases with the distance to the star as $\propto r^{-2}$. This material can be opaque to the propagation of low-frequency photons due to free–free absorption (FFA). Thus, determining the size of the wind photosphere is crucial for interpreting the radio observations.

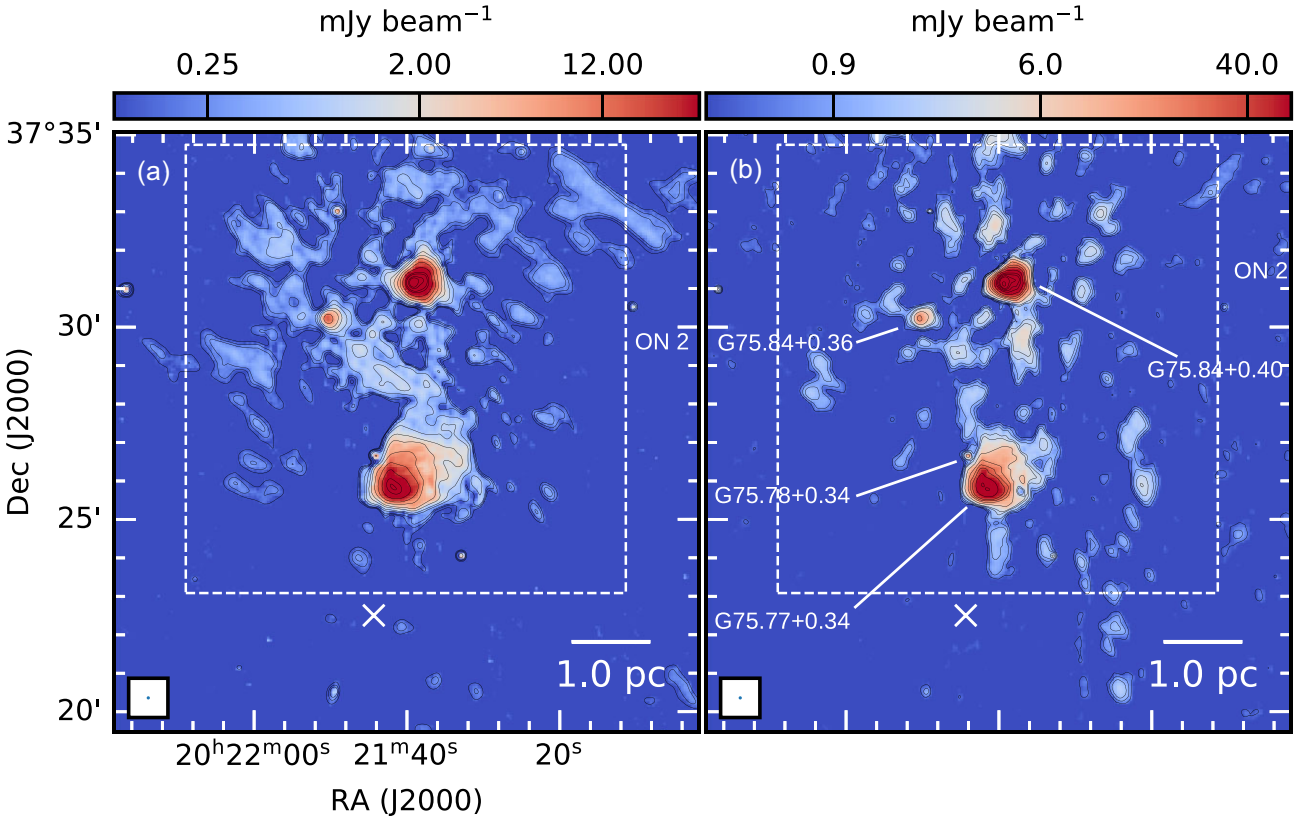

Figure 2. Radio maps of the region around WR 142 obtained using uGMRT GWB data. Both maps are convolved to a circular beam of size 5.0 arcsec. For both panels, the white cross (×) marks the position of WR 142. (a) Map at Band 4 with contour levels of 0.1, 0.2, 0.3, 0.5, 0.9, 1.8, 3.2, 7.0, 14.0, 28.0, 49.0, 57.8, 70.0, 73.5 mJy beam^{-1}. (b) The same but for Band 5 with contour levels of 0.4, 0.7, 1.2, 2.2, 3.0, 7.2, 15.6, 24.7, 36.4, 65.0, 114.4, 149.5, 184.6, 208.0, 245.7 mJy beam^{-1}. For both the panels, the contours are smoothed over 5 pixels using a Gaussian kernel. The box shows the approximate extent of the massive star forming region ON 2 with the positions of the identified H II regions marked.

Table 3. Flux density measurements of WR 114 and WR 142.

Wavelength (cm)	Frequency (GHz)	Resolution (arcsec × arcsec)	S_ν (mJy)	Ref
		WR 114		
3	10	1 × 1	<0.45	1
3.6	8.3	9 × 6	0.15	2
6	5	2 × 2	<0.45	1
		3.5 × 3.5	<0.3	3
13	2.3	8 × 5	<0.54	1
20	1.5	12 × 8	<1.17	1
23.8	1.26	2.7 × 1.6	<0.066	This work
40.8	0.735	4.3 × 3.4	<0.123	This work
		WR 142		
3.6	8.3	9 × 6	<0.9	2
6	5	1.2 × 1.2	<0.6	3
23.8	1.26	2.3 × 1.8	<0.096	This work
40.8	0.735	4.1 × 3.3	<0.111	This work

Note. **References.** (1) Chapman et al. (1999); (2) Cappa et al. (2004); (3) Abbott et al. (1986).

We define the effective radius R_ν that corresponds to an optical depth of unity at a frequency ν. This determines the minimum size from which radiation observed at a frequency ν can originate, as beyond R_ν the wind material is optically thin and contributes to the total emission received. The characteristic radius of free–free emission region for a spherically symmetric wind of a star with a uniform mass-loss rate $\dot{M}$ and terminal velocity v_∞ can be expressed as (Wright & Barlow 1975; Daley-Yates, Stevens & Crossland 2016)

$$\left[\frac{R_\nu}{\mathrm{cm}}\right] = 1.75\times10^{28}\gamma^{1/3}Z^{2/3}g_{\mathrm{ff}}^{2/3}T_{\mathrm{e}}^{-1/2} \times\left(\left[\frac{\dot{M}}{\mathrm{M_\odot\,yr^{-1}}}\right]\left[\frac{\mathrm{km\,s^{-1}}}{v_\infty}\right]\frac{1}{\sqrt{f_{\mathrm{w}}}\,\mu\nu}\right)^{2/3}, \quad (1)$$

where the free–free Gaunt factor (g_{ff}) can be approximated as (Leitherer & Robert 1991)

$$g_{\mathrm{ff}} = 9.77\left(1+0.13\log\frac{T_{\mathrm{e}}^{3/2}}{Z\nu}\right). \quad (2)$$

In these equations, f_{w} is the volume filling factor which takes into account the stellar wind clumping (Puls, Vink & Najarro 2008); T_{e} is the electron temperature of the wind; μ, Z, and γ are the mean molecular weight, the *rms* ionic charge, and the mean number of electrons per ion, respectively. Taking the values of $\dot{M}$, and v_∞ from Table 1, and considering $T_{\mathrm{e}} \approx 0.3\,T_*$ at radius much greater that R_* (see Drew 1990), $f_{\mathrm{w}} = 0.2$, $\mu = 4.0$, $Z = 1.005$, and $\gamma = 1.01$ (Leitherer, Chapman & Koribalski 1995), we calculate the effective radii of the stellar wind photosphere for WR 114 and WR 142 as a function of frequency. At the uGMRT frequencies of 735 and 1260 MHz (the effective frequencies of Bands 4 and 5, respectively), $R_\nu(\tau_{\mathrm{ff}} = 1)$ is estimated to be 104 and 71 AU, respectively for WR 114, and 34 and 23 AU, respectively for WR 142. Taking the distance estimates, these translate to angular sizes of 0.05

and 0.04 arcsec for WR 114, and 0.02 and 0.014 arcsec for WR 142, respectively. Comparing with the resolution of the maps (see Table 2), the stellar wind photosphere would be unresolved in the uGMRT maps, and thus the emission from the stellar winds would be point-like. In addition, we can expect that any emission from the direct surroundings of the WR stars within these photospheric radii will be severely free–free absorbed.

4.2 Interpreting radio non-detection

Over the last few decades, investigation of large samples of systems containing OB and WR stars (e.g. Abbott et al. 1986; Leitherer et al. 1995, 1997; Chapman et al. 1999; Cappa et al. 2004; Montes et al. 2009; De Becker & Raucq 2013) and studies of individual targets (e.g. Williams et al. 1997; Benaglia et al. 2005; Dougherty et al. 2005; O'Connor et al. 2005; Benaglia et al. 2010, 2015, 2019; De Becker, Isequilla & Benaglia 2019; Prajapati et al. 2019) have revealed the presence of both thermal and NT radio emission. WR stars are often seen to be in binary (or higher multiplicity) systems (e.g. Meyer et al. 2020). Hence, for the two WR stars studied here, even though there is no conclusive observational evidence of binarity, we cannot rule out this possibility. Consequently, our interpretation of the results obtained from radio observations will consider both scenarios.

4.2.1 *Single stellar systems*

For single WR stellar systems, in principle, the observed radio emission is expected to be due to thermal free–free radiation from the partially optically thick stellar wind with a canonical spectral index $\alpha = 0.6$ (Panagia & Felli 1975; Wright & Barlow 1975). The flux density due to free–free emission ($S_\nu^{\rm ff}$) in the ionized stellar wind of a star with a uniform mass-loss rate, and isothermal outflow with constant wind velocity can be written as (Panagia & Felli1975; Wright & Barlow1975)

$$\left[\frac{S_\nu^{\rm ff}}{\rm Jy}\right] = 23.2 \left(\left[\frac{\dot{M}}{\rm M_\odot\ yr^{-1}}\right]\left[\frac{\rm km\ s^{-1}}{v_\infty}\right]\frac{1}{\sqrt{f_{\rm w}}\,\mu}\right)^{4/3} \times \left(\gamma\, g_{\rm ff} Z^2 \nu \left[\frac{\rm kpc}{D}\right]^3\right)^{2/3}, \quad (3)$$

where D is the distance to the source, and the rest of the parameters have the same meaning as in equation (1). Figs 3(a) and (b) show the predicted radio spectral energy distribution (SED) for the stellar wind of WR 114 and WR 142, respectively. The estimated uGMRT upper limits together with those from the literature (see Table 3) are also plotted in the figures.

For WR 114, considering the predicted flux density values (169.1 μJy at Band 4 and 235.1 μJy at Band 5), there should have been detections at $\sim 4\sigma$ and $\sim 10\sigma$ level in uGMRT Bands 4 and 5, respectively. Similar inferences can be drawn for four of the data points taken from Abbott et al. (1986), Chapman et al. (1999), and Cappa et al. (2004). Hence, the non-detection strongly suggests that either some of the adopted stellar and/or wind parameters are not accurate, or that the assumed stellar wind model is not appropriate for this WR system. The predicted flux density is most sensitive to the mass-loss rate (equation 3). For WR 114, the uGMRT upper limit in Band 5 enables us to constrain the mass-loss rate to $\dot{M} \lesssim 1.2 \times 10^{-5}\,{\rm M_\odot\ yr^{-1}}$. A tighter constrain on $\dot{M} \lesssim 1 \times 10^{-5}\,{\rm M_\odot\ yr^{-1}}$ can be made by using the local *rms* of 18 μJy beam^{-1}. In comparison, for WR 142, the non-detection agrees well with the flux densities predicted by the model. We highlight that mass-loss rates derived from thermal radio emission have been argued to be more accurate and robust than those from complex spectroscopic modelling approach. Estimates from radio emission are mostly based on observable quantities (see equation 3) unlike the other methods which are model-dependent. In fact, radio observations have been widely used to determine or constrain mass-loss rates in massive stars (e.g. Abbott et al. 1986; Cappa et al. 2004; Benaglia et al. 2019; De Becker et al. 2019; Gallego-Calvente et al. 2021; Moutzouri et al. 2022); a comprehensive discussion on the advantages and limitations of different methods can be found in Puls et al. (2008).

Besides, the scenario of NT radio emission associated with single (non-runaway) WR stars deserves to be discussed as well. On the one hand, local instabilities (e.g. Lucy & White 1980; White 1985) or magnetic confinement (e.g. Jardine et al. 2001) have been proposed to give rise to particle acceleration in single stellar winds. However, this has never been confirmed by the numerous radio observations of massive stars over the past decades. On the other hand, the termination shocks of stellar bubbles powered by WR stars are more likely to offer the required conditions to drive efficient particle acceleration. This is seen in the case of the WR bubble G2.4+1.4 around WR 102, where the detection of synchrotron emission was reported by Prajapati et al. (2019) on a bubble of radius ∼2.5 pc. For WR 114, there is no associated stellar bubble detected in the *GLIMPSE*[4] or *WISE*[5] images. The field of WR 142 is comparatively complex. It is located at the edge of a large-scale superbubble/shell associated with Cyg OB1 harbouring multiple WR and Of stars. Lozinskaya (1991) discuss about an infrared shell of ∼3° but rule out the likelihood of its formation due to WR 142 superwind. The formation, size, and lifetime of these bubbles depend on several factors such as the progenitor evolutionary phase, wind parameters, mass ejected in previous evolutionary phases, the local ISM density, lifetime in the WR phase, the proper motion of the star, swept-up matter (ISM or stellar ejecta), and the dissipation rate of wind energy. Observationally, only a small fraction of known Galactic WR stars are seen to be associated with ring nebulae or stellar bubbles (e.g. Lozinskaya 1991; Freyer, Hensler & Yorke 2006). In spite of being similar in spectral type and wind kinematics to WR 102, the WR 142 system does not exhibit any nearby associated stellar bubble. A quantitative comparison is quite difficult given that most of the above-mentioned parameters are unknown for both stars. The non-detection of any wind–ISM interaction regions associated with WR 142 motivates to further investigate the case of WR 102 and the origin of its synchrotron emission.

4.2.2 *Colliding-wind binary (CWB) systems*

WR 114 has been speculated to have a binary companion (van der Hucht 2001). Similarly, the possibility of binary was also suggested for WR 142, in which Sokal et al. (2010) suggested that a colliding-wind shock model – where the wind from the WR star shocks against an undetected companion or its wind – could explain the high temperature indicated by the X-ray spectra. Considering these inferences, in the following analysis we interpret the observational results assuming that both targets are PACWBs.

In PACWBs, low frequency radio emission is most likely to be a combination of (i) free–free emission from the stellar wind of each

[4]Galactic Legacy Infrared Mid-plane Survey Extraordinaire (*GLIMPSE*; Benjamin et al. 2003).
[5]Wide-field Infrared Survey Explorer (*WISE*; Wright et al. 2010).

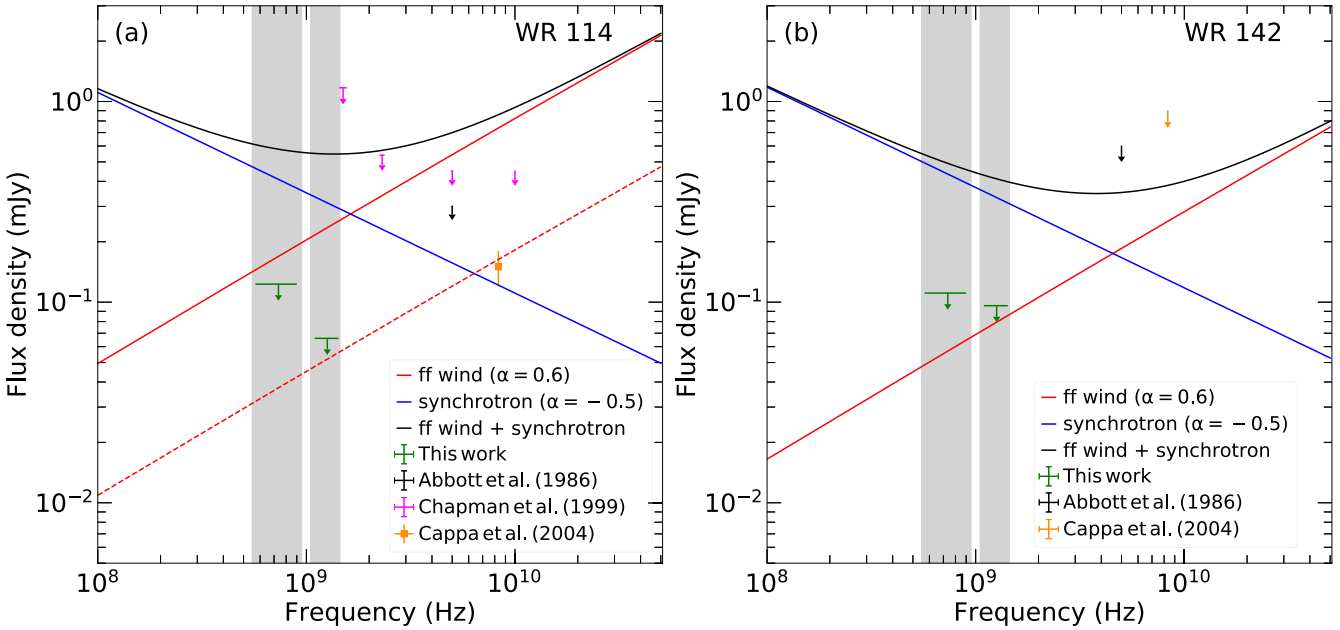

Figure 3. Expected SED of WR 114 (left) and WR 142 (right) at radio frequencies. The red solid line represents the free–free emission from the stellar wind estimated using equation (3) and the parameters listed in Table 1. The blue solid line represents the lower boundary of the predicted flux density for NT emission in CWB system. The combination of these two is shown as black curve. For WR 114, the red dashed line represents the upper boundary of the free–free flux density estimated using $\dot{M} \lesssim 10^{-5}\,\mathrm{M_\odot\,yr^{-1}}$ (see the text in Section 4.2.1). The 3σ upper limits and the flux density values are shown with markers. The shaded regions represent the bands of our radio observations.

binary component, and (ii) synchrotron radiation from the wind-collision region, where relativistic electrons are accelerated. The thermal radiation is expected to follow the free–free emission model discussed in Section 4.2.1. However, estimating the total flux density in these systems is not straightforward.

De Becker & Raucq (2013) discussed the energy budget of stellar winds in PACWBs. In these systems, a fraction of the wind kinetic power is converted to the final radio emission after going through a series of energy conversion processes (see fig. 3 in De Becker & Raucq 2013). Apart from the wind kinetic power and the efficiency of its conversion to particle acceleration giving rise to NT radiation, the observed flux density will also be influenced by FFA that depends on the orbital phase, orientation, and wind opacity. Thus, the radio synchrotron emission is directly proportional to the wind kinetic power, where the proportionality is dependent on several variables that can vary significantly from one system to the other, and as a function of the orbital phase for a specific one.

A radio synchrotron efficiency (RSE) parameter that essentially gives the fraction of wind kinetic power converted to radio emission is defined as (De Becker & Raucq 2013; De Becker et al. 2017)

$$\mathrm{RSE} = \frac{L_{\mathrm{radio}}}{P_{\mathrm{kin}}}. \tag{4}$$

With the census of radio measurements and the information of P_{kin} from the PACWB catalogue of De Becker & Raucq (2013), and based on a few selected objects, De Becker et al. (2017) proposed empirical expressions to estimate the lower and upper boundary of RSE through a quadratic regression (see fig. 4 in De Becker & Raucq 2013). These equations essentially outline the upper and lower limits of RSE as a function of P_{kin}. Subsequently, these can be translated to the expected range of radio luminosities for a system with known P_{kin}. The estimated RSE ranges from $10^{-9.7}$ to $10^{-7.6}$ and $10^{-9.9}$ to $10^{-7.8}$ for WR 114 and WR 142, respectively. The radio luminosity (L_{radio}) is estimated from the RSE limits, which can then be converted to flux density using the following equation:

$$S_\nu^{\mathrm{NT}} = \frac{10^{26}\,(\alpha+1)\,\nu^\alpha\,L_{\mathrm{radio}}}{4\pi\,D^2\,(\nu_2^{(\alpha+1)} - \nu_1^{(\alpha+1)})} \quad \mathrm{mJy}, \tag{5}$$

where S_ν^{NT} is the flux density from NT emission at the observing frequency (ν in Hz), α is the spectral index, and D is the distance to the source expressed in cm. Using the lower limit of radio luminosity, $\nu_1 = 0.1$ GHz, $\nu_2 = 50$ GHz, and adopting $\alpha = -0.5$ (canonical value for synchrotron radiation from relativistic electrons accelerated by DSA in high Mach number adiabatic shocks), we estimate the lower limit of the flux density at different frequencies ν. The resulting SEDs including free–free and synchrotron emission are shown in Fig. 3.

For both sources, the (minimum) expected value is much higher than the 3σ upper limits from our observations. For WR 114, the expected total flux densities are 0.58 and 0.55 mJy at 735 and 1260 MHz, respectively. And in the case of WR 142, at 735 and 1260 MHz, the flux density values are 0.50 and 0.41 mJy, respectively. Thus, if NT emission were present, it should have been detected with a high signal-to-noise ratio in our uGMRT observations. We note that this inference holds also if one assumes a spectral index $\alpha < -0.5$ in the calculation, as seen in some PACWBs (De Becker & Raucq 2013). The non-detection in the lower frequency uGMRT bands, which are ideal for probing NT emission, implies an exceptionally low RSE (RSE $< 10^{-10}$). This opens up a few possibilities that are briefly discussed below:

(i) The stars are not in binary systems with a massive companion with strong winds, leading to a lack of magnetohydrodynamic shocks with the required properties for particle acceleration.

(ii) The stars are in very wide binary systems (with period of decades). In a CWB, the emission from the wind-collision region depends on the stellar separation. In systems with eccentric orbits, the (intrinsic) synchrotron emission peaks towards periastron, when the stellar separation is the least. It is possible that the two WR stars

are in a very long-period orbit, with one of the binary components far from the periastron, leading to a very low synchrotron luminosity.

(iii) The stars are in close binary systems. The wind-collision region would be within the high opacity zone of the radio photospheres of the binary components (see Section 4.1), so that radio emission would be drastically reduced due to FFA. From the estimated stellar wind photospheres, the orbital separation would be less than 70 AU and 20 AU for WR 114 and WR 142, respectively. This is remarkably consistent with the analysis of X-ray observations of WR 142 by Sokal et al. (2010), who showed that the presence of a close (separation of ∼1 AU) B0V companion can explain the observed X-ray luminosity in a colliding-wind shocks scenario. A similar scenario has also been inferred for WR 133 (De Becker et al. 2019) and WR 11 (Benaglia et al. 2019), where the high optical depth zone is much larger than the typical dimension of the full binary system.

5 CONCLUSIONS

We carried out a low-frequency (735 and 1260 MHz) radio continuum study of two WR stars, WR 114 and WR 142, using uGMRT observations with high angular resolution and sensitivity. At both frequencies, no radio emission is detected from either of the WR stars. Based on the non-detection, we report on 3σ upper limits to the radio flux densities at 735 and 1260 MHz (123 and 66 μJy for WR 114, and 111 and 96 μJy for WR 142, respectively). These limits are discussed in the context of two scenarios: stellar wind from a single star and a CWB system.

Considering the thermal emission from the stellar wind of a single star enables us to constrain the mass-loss rate of WR 114 to $\dot{M} \lesssim 10^{-5}\,\mathrm{M_\odot\,yr^{-1}}$, which is a factor of ∼3 lower than the model-based value from Sander et al. (2019). In addition, our analysis does not reveal any synchrotron emission associated to a potential wind–ISM interaction. A comparison to the synchrotron-emitting WR bubble around WR 102 points to the requirement to carefully consider the properties of the direct circumstellar environment to envisage significant particle acceleration at a termination shock.

If we rather assume both WR stars to be in CWB systems, the non-detection of NT emission in the lower frequency uGMRT maps suggests either (i) a very wide binary system (with an orbital period of several decades) not close to periastron, or (ii) a close binary system with strong FFA. Alternatively, the non-detection of synchrotron emission may also indicate the lack of a companion. The latter point deserves complementary studies at other wavebands to independently constrain the multiplicity of these two WR stars.

The investigation of particle acceleration from massive stars in various configurations, either single stars or in binary/multiple systems, definitely deserves to be pushed forward with more targets investigated at various radio frequencies, at various epochs, and keeping track of all potential shock physics scenarios likely to occur in these objects. Our results show that the availability of a quite high kinetic power is not sufficient to warrant the identification of clear indicators of particle acceleration in these objects. In particular, for isolated WR stars, the efficiency of converting wind kinetic power into particle acceleration can be rather low under unfavourable conditions.

ACKNOWLEDGEMENTS

We thank the referee for valuable suggestions that helped us to improve the manuscript. This work was carried out in the framework of the PANTERA-Stars (https://www.astro.uliege.be/~debecker/pantera/) initiative. We thank the staff of the GMRT that made these observations possible. GMRT is run by the National Centre for Radio Astrophysics of the Tata Institute of Fundamental Research.

DATA AVAILABILITY

The raw data is publicly available in the GMRT webpage (https://naps.ncra.tifr.res.in/goa/data/search). The calibrated data used in this article will be shared upon reasonable request to the corresponding author.

REFERENCES

Abbott D. C., Beiging J. H., Churchwell E., Torres A. V., 1986, ApJ, 303, 239
Barlow M. J., 1982, in De Loore C. W. H., Willis A. J., eds, Wolf-Rayet Stars: Observations, Physics, Evolution, Vol. 99. Reidel, Dordrecht, p. 149
Benaglia P., Romero G. E., Koribalski B., Pollock A. M. T., 2005, A&A, 440, 743
Benaglia P., Romero G. E., Martí J., Peri C. S., Araudo A. T., 2010, A&A, 517, L10
Benaglia P., Marcote B., Moldón J., Nelan E., De Becker M., Dougherty S. M., Koribalski B. S., 2015, A&A, 579, A99
Benaglia P., del Palacio S., Ishwara-Chandra C. H., De Becker M., Isequilla N. L., Saponara J., 2019, A&A, 625, A99
Benaglia P., del Palacio S., Hales C., Colazo M. E., 2021, MNRAS, 503, 2514
Benjamin R. A. et al., 2003, PASP, 115, 953
Blumenthal G. R., Gould R. J., 1970, Rev. Mod. Phys., 42, 237
Brogan C. L., Gelfand J. D., Gaensler B. M., Kassim N. E., Lazio T. J. W., 2006, ApJ, 639, L25
Cappa C., Goss W. M., van der Hucht K. A., 2004, AJ, 127, 2885
Chapman J. M., Leitherer C., Koribalski B., Bouter R., Storey M., 1999, ApJ, 518, 890
Daley-Yates S., Stevens I. R., Crossland T. D., 2016, MNRAS, 463, 2735
De Becker M., Raucq F., 2013, A&A, 558, A28
De Becker M., Benaglia P., Romero G. E., Peri C. S., 2017, A&A, 600, A47
De Becker M., Isequilla N. L., Benaglia P., 2019, A&A, 623, A163
del Palacio S., García F., De Becker M., Altamirano D., Bosch-Ramon V., Benaglia P., Marcote B., Romero G. E., 2023, A&A, 672, A109
Dougherty S. M., Beasley A. J., Claussen M. J., Zauderer B. A., Bolingbroke N. J., 2005, ApJ, 623, 447
Drew J. E., 1990, ApJ, 357, 573
Drury L. O., 1983, Rep. Prog. Phys., 46, 973
Eldridge J. J., Langer N., Tout C. A., 2011, MNRAS, 414, 3501
Freyer T., Hensler G., Yorke H. W., 2006, ApJ, 638, 262
Gabici S., 2023, preprint (arXiv:2301.06505)
Gaia Collaboration 2023, A&A 674, A1
Gallego-Calvente A. T. et al., 2021, A&A, 647, A110
Green D. A., 2009, Bull. Astron. Soc. India, 37, 45
Gupta Y. et al., 2017, Curr. Sci., 113, 707
Hamann W. R., Koesterke L., Gräfener G., 2000, in Lamers H., Sapar A., eds, ASP Conf. Ser. Vol. 204, Thermal and Ionization Aspects of Flows from Hot Stars. Astron. Soc. Pac., San Francisco, p. 197
Jardine M., Collier Cameron A., Donati J. F., Pointer G. R., 2001, MNRAS, 324, 201
Kale R., Ishwara-Chandra C. H., 2021, Exp. Astron., 51, 95
Kingsburgh R. L., Barlow M. J., Storey P. J., 1995, A&A, 295, 75
Leitherer C., Robert C., 1991, ApJ, 377, 629
Leitherer C., Chapman J. M., Koribalski B., 1995, ApJ, 450, 289
Leitherer C., Chapman J. M., Koribalski B., 1997, ApJ, 481, 898
Lozinskaya T. A., 1991, in van der Hucht K. A., Hidayat B.eds, Wolf-Rayet Stars and Interrelations with Other Massive Stars in Galaxies, Vol. 143. Springer, Dordrecht, p. 365
Lucy L. B., White R. L., 1980, ApJ, 241, 300
McMullin J. P., Waters B., Schiebel D., Young W., Golap K., 2007, in Shaw R. A., Hill F., Bell D. J.eds, ASP Conf. Ser. Vol. 376, Astronomical Data

Analysis Software and Systems XVI. Astron. Soc. Pac., San Francisco, p. 127
Meyer D. M. A., Oskinova L. M., Pohl M., Petrov M., 2020, MNRAS, 496, 3906
Montes G., Pérez-Torres M. A., Alberdi A., González R. F., 2009, ApJ, 705, 899
Moutzouri M. et al., 2022, A&A, 663, A80
Nugis T., Lamers H. J. G. L. M., 2000, A&A, 360, 227
Nugis T., Crowther P. A., Willis A. J., 1998, A&A, 333, 956
O'Connor E., Dougherty S., Pittard J., Williams P., 2005, J. R. Astron. Soc. Canada, 99, 142
Oskinova L. M., Ignace R., Hamann W. R., Pollock A. M. T., Brown J. C., 2003, A&A, 402, 755
Panagia N., Felli M., 1975, A&A, 39, 1
Pavlović M. Z., Urošević D., Vukotić B., Arbutina B., Göker Ü. D., 2013, ApJS, 204, 4
Perley R. A., Butler B. J., 2017, ApJS, 230, 7
Pittard J. M., Romero G. E., Vila G. S., 2021, MNRAS, 504, 4204
Prajapati P., Tej A., del Palacio S., Benaglia P., CH I.-C., Vig S., Mandal S., Kanti Ghosh S., 2019, ApJ, 884, L49
Puls J., Vink J. S., Najarro F., 2008, A&AR, 16, 209
Rau U., Cornwell T. J., 2011, A&A, 532, A71
Sander A., Hamann W. R., Todt H., 2012, A&A, 540, A144
Sander A. A. C., Hamann W. R., Todt H., Hainich R., Shenar T., Ramachandran V., Oskinova L. M., 2019, A&A, 621, A92
Seo J., Kang H., Ryu D., 2018, J. Korean Astron. Soc., 51, 37
Smith L. F., 1968, MNRAS, 138, 109
Sokal K. R., Skinner S. L., Zhekov S. A., Güdel M., Schmutz W., 2010, ApJ, 715, 1327
Swarup G., Ananthakrishnan S., Kapahi V. K., Rao A. P., Subrahmanya C. R., Kulkarni V. K., 1991, Curr. Sci., 60, 95
van der Hucht K. A., 2001, New Astron. Rev., 45, 135
White R. L., 1985, ApJ, 289, 698
Williams P. M., Dougherty S. M., Davis R. J., van der Hucht K. A., Bode M. F., Setia Gunawan D. Y. A., 1997, MNRAS, 289, 10
Wright A. E., Barlow M. J., 1975, MNRAS, 170, 41
Wright E. L. et al., 2010, AJ, 140, 1868

This paper has been typeset from a TEX/LATEX file prepared by the author.